Journal of Geointerface, Vol. 4, No. 2, December 2025, pp. 1–14 e-ISSN: 2583-6900

# Compositional diversity of spinel-magnetite association in the metapelites of the Kerala Khondalite Belt, southern India

Resmi S. [1,2], Shaji E. [1,*], Dhanil Dev S.G. [1]

[1] *Department of Geology, University of Kerala, Kariavattom campus, Thiruvananthapuram 695 581, India*
[2] *Geological Survey of India, Northern Region, Lucknow 226 024, India*

## ABSTRACT

The Kerala Khondalite Belt (KKB), preserves high-temperature metamorphic rocks that record a complex polymetamorphic history. This study focuses on the textural and compositional characterization of spinel–magnetite associations in metapelites from the KKB. Petrographic investigations reveal that spinel and magnetite occur as inclusions within garnet and cordierite, at grain boundaries, and occasionally as exsolution features. Electron Probe Micro-Analyzer (EPMA) data indicate that spinel compositions range from hercynite- to pleonaste-dominated varieties, with low $Cr_2O$ (<0.7 wt%) and variable ZnO (0.3–1.6 wt%) and MgO (7–15 wt%), suggesting Al-rich, Cr-poor spinels typical of high-temperature metapelitic environments. Magnetite shows near-end member $Fe\,O_4$ compositions with minor Ti, Al, and Cr substitutions. End-member modeling confirms a dominant hercynite component in spinel, with minor gahnite and spinel sensu stricto. Magnetite is enriched in ulvöspinel, pointing to partial Ti substitution and post-peak exsolution processes. Binary cation plots exhibit a negative correlation between $Al^{3+}$ and $Fe^{3+}$ and between $Mg^{2+}$ and $Fe^{2+}$ in spinel, reflecting coupled Fe–Mg–Al substitutions during metamorphism. ZnO content shows an increasing trend away from the Achankovil Shear Zone (ASZ). Garnet–cordierite geothermometry yields retrograde temperatures of 731–751 °C and pressures of ∼4.6–4.8 kbar, confirming cooling following Ultra High Temperature (UHT) conditions. The occurrence of magnetite at spinel grain boundaries or within garnet, and the development of corona textures between garnet and spinel, reflect redox-sensitive reactions and partial retrogression. These textures, along with compositional zoning, provide compelling evidence for oxidation-driven magnetite formation during decompression and cooling. The spinel–magnetite association thus serves as a powerful proxy for deciphering the redox evolution, reaction pathways, and P–T history of the KKB metapelites.

**ARTICLE HISTORY**

Received: 07 May 2025
Revised: 02 June 2025
Accepted: 04 June 2025

https://doi.org/10.5281/zenodo.15623276

**KEYWORDS**

Spinel
Magnetite
Pleonaste
Kerala Khondalite Belt
Metapelites

*Corresponding author. Email: shajigeology@keralauniversity.ac.in (SE), georesmi07@gmail.com (RS), dhanildev@keralauniversity.ac.in (DDSG)

 

## 1. Introduction

The spinel group of minerals serve as valuable indicators of the geological conditions present during the formation of their host rocks. Many studies use this assemblage as an excellent marker for identifying petrogenesis and tectonic settings (Mahanta et al., 2025; Nugumanova et al., 2024; Power et al., 2000) including Kerala Khondalite Belt (KKB). This study focuses on the spinel-bearing metapelites of KKB (Fig. 1) and its association with magnetite. Spinel group minerals are common accessory phases in various metamorphic rocks, particularly those formed under high-temperature conditions. Their presence and composition provide valuable insights into the metamorphic grade, pressure-temperature (P–T) paths, and the chemical environment during metamorphism (Harley, 1998). For this reason, spinel-bearing mineral assemblages have confirmed their successful appliance to know the genesis of rocks. Compositionally, igneous spinel is typically rich in chromium. Whereas, spinel of metamorphic origin contain higher iron and magnesium concentrations is observed with increasing metamorphism and alteration. In general, the genesis of spinel is associated with two distinct metamorphic environments: (i), the contact metamorphism of calcium-rich lithologies (Loomis, 1972; Atkin, 1978), and (ii) the high-grade regional metamorphism of limestone and pelitic rock suites (Frost, 1973; Wagner and Crawford, 1975).

Spinel-bearing metapelites, indicative of high-grade metamorphism, have been the subject of extensive study across various orogenic belts worldwide (Navrotsky and Kleppa, 1968; Tadokoro et al., 2007; Wang et al., 2021; Aung and Nyunt, 2021; Ouzegane et al., 2025). Research has focused on understanding the pressure-temperature (P–T) conditions, metamorphic reactions, and fluid interactions that govern spinel stability and composition. In the Grenville Province of North America, studies have detailed the occurrence of hercynite-rich spinel in association with cordierite and sillimanite, constraining peak metamorphic temperatures and pressures (Herd et al., 1987). Similarly, investigations in the KKB of India have documented the presence of Mg–Al spinel in metapelites, providing insights into ultrahigh temperature metamorphism (Tadokoro et al., 2008, Shimizu et al., 2009). Research in the Bohemian Massif has explored the relationship between spinel composition and the activity of components such as ZnO, influencing phase equilibria (Tajčmanová et al., 2009). These studies, employing petrography, mineral chemistry, and thermobarometry, collectively contribute to a broader understanding of metamorphic processes and the evolution of crustal rocks under extreme conditions.

As the southernmost segment of the Southern Granulite Terrain (SGT), the KKB (Fig. 1) exhibits evidence of high-grade metamorphism, reaching high to ultrahigh temperatures (Chacko et al., 1987; Harley, 1998) during the Pan-African period. This area of polymetamorphism is a component of a significant Meso-Neoproterozoic mobile zone and is composed of supracrustal lithologies (Srikantappa et al., 1985; Ramakrishnan, 1993). The predominant rock types include quartzo-feldspathic gneisses containing garnet and biotite, metapelites rich in sillimanite and graphite, and garnet-cordierite (with or without orthopyroxene) granulites. Spinel-bearing assemblages have proven vital for understanding the metamorphic pressure-temperature (P–T) conditions in the KKB. Notably, the reported occurrence of spinel alongside quartz in khondalites (garnet-sillimanite-biotite ± cordierite gneiss) is a key indicator. This specific mineral association suggests very high temperatures, generally above 900 °C at moderate pressures, as evidenced by multiple investigations (Morimoto et al., 2004; Tadokoro et al., 2008; Kadowaki et al., 2019). Magnetite is reported as part of the mineral assemblage in several rock types within the KKB. In felsic to intermediate granulites, the peak metamorphic assemblage can include magnetite. Studies on charnockites (orthopyroxene-bearing quartzo-feldspathic gneisses) in the KKB have mentioned the presence of magnetite along with other minerals like orthopyroxene, garnet, K-feldspar, plagioclase, biotite, and quartz. While both spinel and magnetite are known constituents of the KKB, existing literature lacks a specific focus on their direct textural relationship as a key indicator of metamorphic conditions or reactions, in contrast to the well-established spinel + quartz assemblage (Shimizu et al., 2009). The current study addresses this gap by detailing occurrences of spinel-magnetite association in KKB metapelites and presenting a comparative analysis of their mineral chemistry based on Electron Probe Microprobe Analyzer (EPMA) analysis. The observed coexistence of spinel and magnetite suggests metamorphic conditions distinct from those inferred from other assemblages in these metapelites.

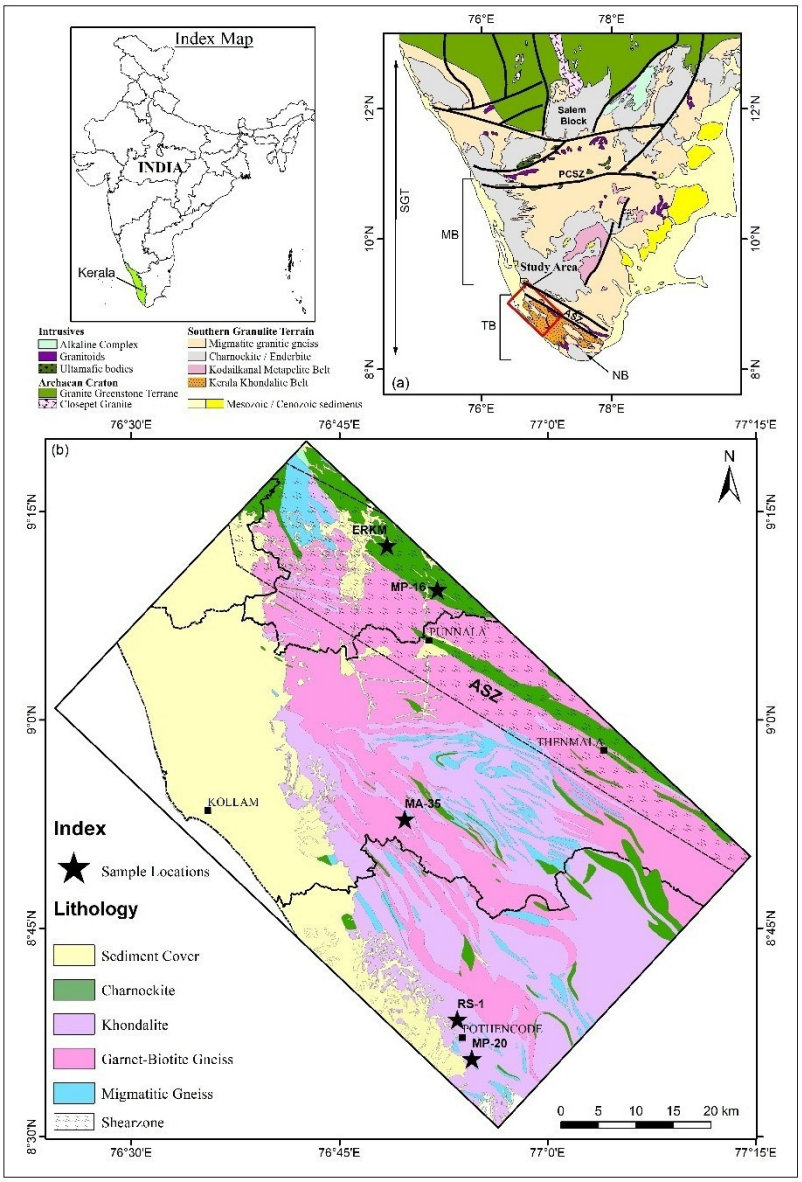


Fig. 1. (a) Simplified geological sketch of southern India showing the Southern Granulite terrane; (b) Modified geological map of the study area showing different lithologies and sampling locations (Data Source: GSI, Bhukosh, 1: 50,000; SGT: Southern Granulite Terrain, MB: Madurai Block; TB: Trivandrum Block; NB: Nagercoil Block PCSZ: Palghat–Cauvery shear zone, ASZ: Achankovil Shear Zone).

## 2. Regional geology

The SGT, representing the southernmost part of the Indian Shield, has been conventionally subdivided into crustal blocks delineated by roughly east-west striking shear zones. Within its Kerala segment, the Palghat Cauvery Shear Zone (PCSZ) is situated in the Palghat Valley, with the Madurai Block (MB) lying south. The Karur–Kambam–Painavu–Trissur lineament traverses the MB, while the Achankovil Shear Zone (ASZ) marks a significant structural boundary between the MB and the Trivandrum Block (TB, Fig. 1). South of the PCSZ, two principal domains are recognized: the MB in the north and the KKB in the south, which encompasses the Trivandrum Block and the ASZ. The KKB is one of South India's largest granulite-facies supracrustal terrains. A northwest-southeast trending shear zone, the ASZ define its northern boundary. The KKB is composed of a supracrustal sequence, intrusive granitoids, and abundant charnockite, all intensely deformed into gneisses (Ramakrishnan, 1993; Chacko et al., 1987; Bindu et al., 1998). The lithology of the KKB is dominated by highly migmatitic garnet-cordierite-biotite-sillimanite gneiss, garnet-biotite augen gneiss,

garnet-biotite leptinitic gneiss, and cordierite-garnet-orthopyroxene gneiss. A pervasive feature throughout the KKB is the extensive migmatization resulting from biotite dehydration melting (Braun et al., 1996; Cenki et al., 2004). Notably, the KKB exhibits widespread charnockitization of pre-existing quartzofeldspathic gneisses (Kumar et al., 1985; Kumar and Sreejith, 2016).

This study investigates the geology and geochemistry of metamorphic rocks from the Kerala segment of the KKB. Samples were collected from readily accessible, active quarries, providing an excellent opportunity to sample a significant portion of the KKB's supracrustal rocks across a wide area (Fig. 1). The rocks in the study area are well-jointed and show a general foliation trend of N40°W with varying dip towards SW. The major rock types of the study area are cordierite gneiss, garnetiferous biotite gneiss, charnockite and pyroxene granulite.

*Garnetiferous Biotite Gneiss (GBG):* GBG unit is leucocratic, medium-grained, well-jointed, containing small biotite flakes and uniformly distributed, minimally porphyroblastic garnet (Fig. 2b). In the study area gneissic fabric is seen as alternate bands of light coloured minerals like quartz and feldspar and dark coloured aggregates of micaceous minerals, cordierite and garnet. Thin, dark biotite-rich bands with sharp contacts are present. At some places presence of pegmatite vein with large quartz, feldspar, biotite, and garnet crystals contains charnockite patches, indicating syn-metamorphic charnockite development within both the GBG and the pegmatite. At some places highly migmatized rocks show distorted foliation, rotated and sheared garnet porphyroblasts (some up to 12 cm, wrapped by sillimanite).

*Cordierite Gneiss:* Cordierite gneiss in the study area is greyish-white with a characteristic bluish sheen. This medium- to coarse-grained gneiss contains aligned, lenticular cordierite porphyroblasts (up to 10 cm) and displays gneissic to schistose banding with variable mineral proportions (Fig. 2a). The rock exhibits gneissic structure although in a number of outcrops it shows schistose bands. The proportion of mineral content differs considerably even within the same outcrop. Key minerals are cordierite (Crd), garnet (Grt), sillimanite (Sil), graphite, quartz (Qz), and Plagioclase feldspar (Pl), exhibiting a granoblastic texture and compositional layering. The gneiss is leucocratic and banded (light: quartz-feldspar; dark: cordierite-biotite), with foliation parallel to the banding. Cordierite is the most abundant mineral, followed by quartz, feldspar, garnet, sillimanite, and biotite. Cordierites are distinguished by its bluish colour, vitreous luster and subconchoidal fracture. At places they are altered to pinnite. Quartz grains are identified by their fresh appearance, vitreous luster, conchoidal fracture, lack of cleavage. Feldspars are distinguished by their white to grey colour, subvitreous luster and good prismatic cleavage. Garnet grains are identified by their pink to reddish colour, subvitreous lustre, subconchoidal fracture and very high hardness. At places they form porphyroblasts and are wrapped up by sillimanite grains. Garnet grains vary in size. Sillimanite grains are recognized by its fibrous nature, vitreous lustre and prismatic cleavage. Biotite is identified by its flaky habit, brownish black colour, pearly lustre, transparency, perfect basal cleavage and low hardness.

*Charnockite*: Charnockite present in the study area are dark (greenish grey to bluish black) coloured, medium to coarse grained and equigranular. It is a hypersthene-bearing rock exhibiting granulitic texture. The rock is mainly composed of feldspar, quartz, biotite and feldspar. The presence of cordierite in the charnockites are observed in the Kollam and Pathanamthitta Districts. A number of varieties of charnockite were noticed in the study area, massive charnockite, gneissic charnockite and patchy charnockite.

## 3. Petrography

In this section we briefly summarize the salient petrographic features of representative rocks from the the selected five locations (Fig. 1, Koliyakod (MP-20); Kanjampara (RS-1); Kannankod (MA-35); Pakkandom (MP-16); Chandanapally Estate (ERKM)). The textural characteristics of these rocks are shown in Fig. 2. The main focus of the present study is to identify the compositional variation in the spinel (Spl) and its associated magnetite (Mag). Detailed petrographic study of the thin section prepared for the samples shows that in the area under investigation spinel and magnetite are usually found to occur in two groups: one as inclusion within garnet and another in association with cordierite from the metapelites. Spinel group of minerals are found occur as small patches within the cordierite gneiss units and are usually found as inclusions within the mesosome layer within the migmatites (Fig. 2a, b).

 

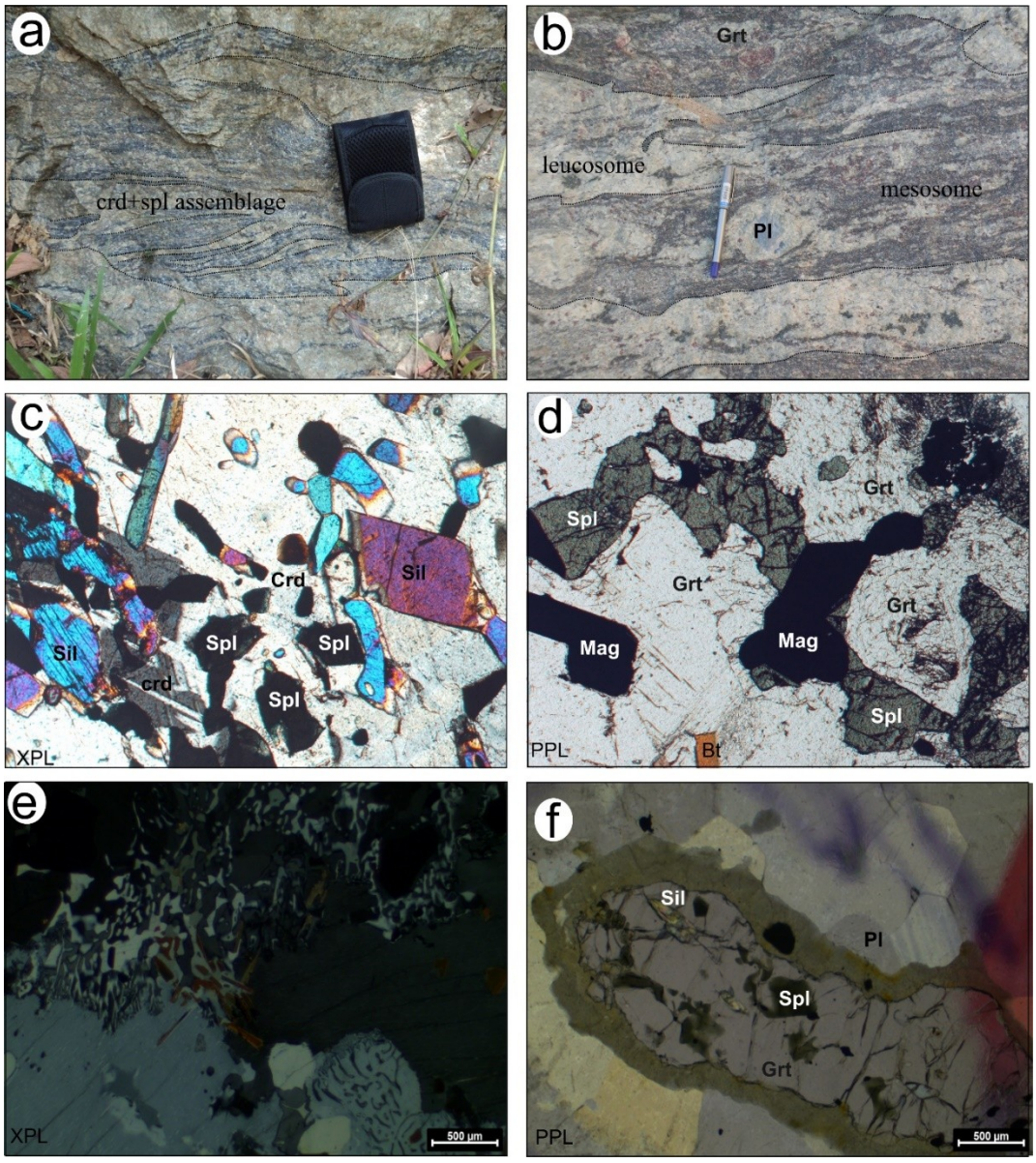


Fig. 2. (a) Field photograph of cordierite-spinel assemblages from Cordierite Gneiss of Punalur area. (b) Layers showing leucosome and mesosome from spinel-bearing metapelites assemblages from Koliyakod. (c) Photomicrographs of spinel-magnetite-cordierite-sillimanite-quartz association in khondalites (d) Photomicrograph of spinel-magnetite-biotite-quartz as inclusions within garnet porphyroblast from migmatites. (e) symplectitic texture of quartz, feldspar and biotite in the migmatites (f) Reaction coronas around garnet grains surrounded by feldspars and cordierite. The garnet is fractured and cordierite is found along the fractures with spinel. (crossed-polar photographs are marked as XPL; plane polarised photographs are marked (PPL)).

Garnetiferous Biotite Gneiss composed dominantly of quartz (30%), plagioclase (15%), garnet (7%) and biotite (5-10%) with accessory K-feldspar, spinel, sillimanite and Magnetite (sample MA-35, ERKM). Garnet and contains numerous fibrous inclusions of sillimanite, biotite, spinel. The inclusion sillimanites are aligned along the matrix foliation. Biotite is present in the matrix. Fine-grained symplectic aggregates of quartz and feldspar occur in the rocks along with biotite (Fig. 2e). Reaction coronas are present around the garnet (Fig. 2f) and complex intergrowth of magnetite and spinel is also found within garnet. Similar microstructure are indications of garnet breakdown during post-peak lower-temperature stage in the same metamorphic cycle (Nandakumar and Harley, 2000). In migmatites garnet is present as porphyroblasts as well as fine to coarse grains which contain inclusions of sillimanite, spinel, magnetite, feldspar. Spinel is present as small randomly oriented grains. Myrmekitic intergrowth

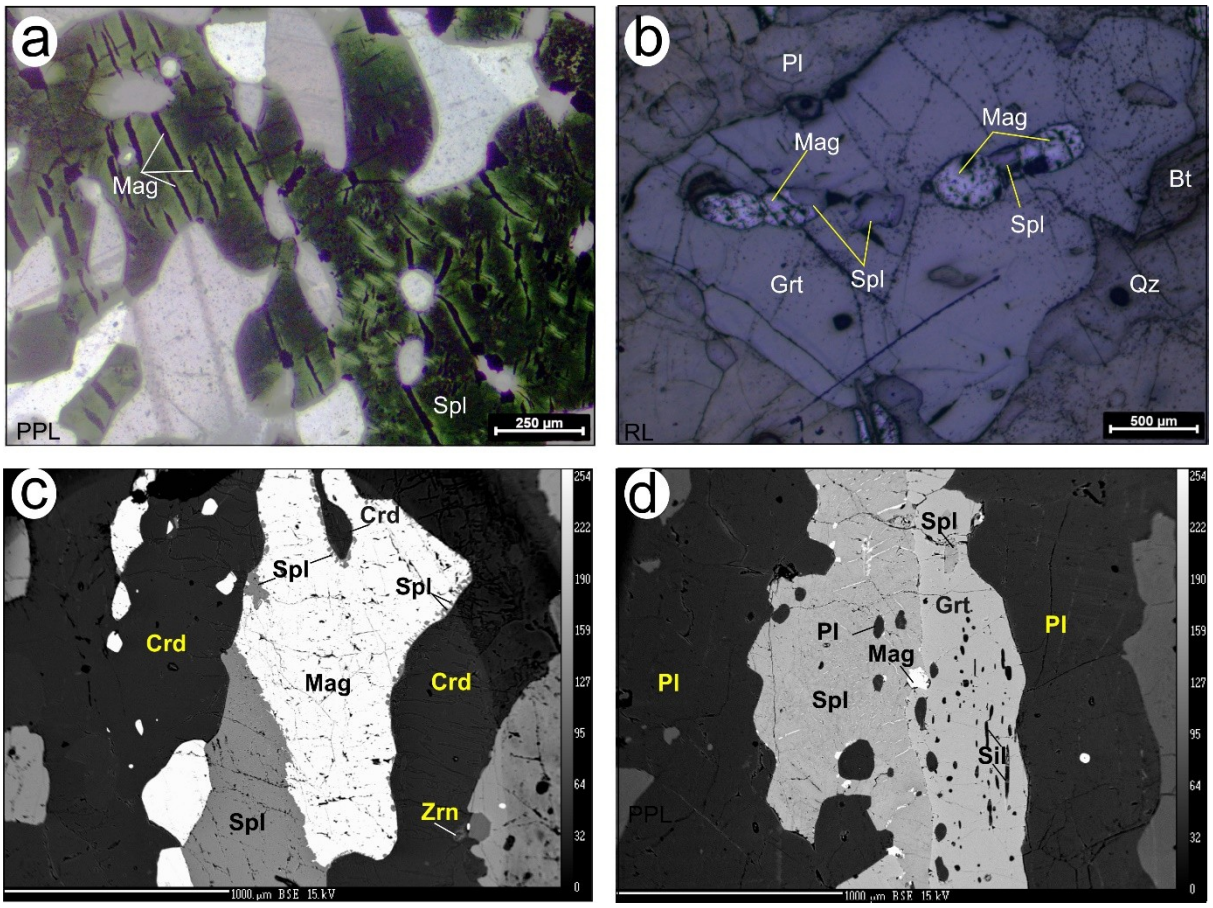


Fig. 3. (a) Photomicrograph of spinel containing resolution patches of magnetite in cordierite gneiss in plane polarised light, (b) Reflected light image of spinel-magnetite association within garnet (c) BSE image showing spinel-magnetite inclusions in cordierite grains within GBG. (d) BSE image of coarse grained plagioclase- fractured spinel- magnetite-garnet association in khondalite.

of feldspar is also common in GBG. Khondalites are characterized by strong schistosity. The mineral assemblages are sillimanite + biotite + garnet + spinel + feldspar + quartz + opaque. The parallel arrangement of biotite and sillimanite develops the schistosity in the rock.

In the study area, spinel and magnetite are subhedral to anhedral in shape, coarse to fine-grained with random orientation (Fig. 2c, 2d, 3a, Fig. 3c, Fig. 3d). Spinel is found occur within the garnet in association with quartz shows garnet formation in upper amphibolite to granulite facies during heating and burial. Prograde mineral reactions based on assemblage identified in this area are:

Spinel + Quartz → Garnet

Biotite + Sillimanite + Quartz → Garnet + K-feldspar + $H_2O$

Cordierite + Quartz → Garnet + Sillimanite + $H_2O$

Magnetite occurs in different forms; as exsolution patches within spinel (Fig. 3a, 3b) and as mineral aggregates (Fig. 3c, 3d). This association is found in most cases associated with garnet. Fe-rich metapelites at granulite facies conditions and moderately oxidizing environments, garnet + spinel + magnetite can coexist stably.

## 4. Mineral Chemistry

To determine the chemical composition of spinel and magnetite of metapelites, EPMA analyses were carried out at EPMA Laboratory, Central Petrological Laboratory, Central Head Quarters, G.S.I., Kolkata by using CAMECA SX-100 Electron Microprobe. EPMA data are represented by the weight percentage of major oxides. Raw data of the spinel group (spinel and magnetite) are processed through the application End-Members Generator (EMG) of Ferracutti et al. (2015). In EMG, the $Fe^{3+}$–$Fe^{2+}$ ratio estimation is carried out according to the methodology of Droop (1987). All the calculations including the $Fe_2O_3$ calculation from FeO (Total),

 

Table 1. Representative mineral chemistry from Spinel and Magnetite from the metapelites of KKB.

| | | | | | | | | | | | | | |
|---|---|---|---|---|---|---|---|---|---|---|---|---|---|
| | | | | | | **Spinel** | | | | | | | |
| Rock Type | | | **Migmatite** | | | **K** | | | **GBG** | | **CG** | | **GBG** |
| Sample No | | | MP-20 | | | RS 1 | | | MA35 | | MP16 | | ERKM | |
| Analysis No | 35 | 36 | 39 | 40 | 3 | 4 | 3 | 4 | 5 | 22 | 2 | 6 | 8 |
| $SiO_2$ | 0 | 0.060 | 0.010 | 0.050 | 0.040 | 0.015 | 0.053 | 0.045 | 0.034 | 0.048 | 0.000 | 0.010 | 0.020 |
| $TiO_2$ | 0 | 0.010 | 0.040 | 0 | 0 | 0.038 | 0.013 | 0.029 | 0 | 0.019 | 0.010 | 0 | 0 |
| $Al_2O_3$ | 59.110 | 59.580 | 57.060 | 59.740 | 60.033 | 60.436 | 63.766 | 63.698 | 63.757 | 60.452 | 59.990 | 59.760 | 60.090 |
| $Cr_2O_3$ | 0.130 | 0.060 | 0.120 | 0.140 | 0.742 | 0.638 | 0.180 | 0.173 | 0.191 | 0.172 | 0.420 | 0.520 | 0.500 |
| FeO | 29.440 | 28.900 | 31.000 | 28.930 | 31.269 | 31.415 | 18.422 | 17.991 | 17.739 | 29.606 | 28.970 | 29.810 | 29.160 |
| MnO | 0.510 | 0.570 | 0.440 | 0.590 | 0.116 | 0.057 | 0.066 | 0.095 | 0.050 | 0.581 | 0.000 | 0.060 | 0.030 |
| MgO | 9.390 | 9.740 | 9.060 | 9.960 | 7.292 | 7.114 | 14.702 | 14.889 | 14.970 | 9.245 | 9.580 | 9.370 | 9.460 |
| CaO | 0.010 | 0.020 | 0.060 | 0.000 | 0.000 | 0.000 | 0.006 | 0.000 | 0.000 | 0.000 | 0.010 | 0.020 | 0.000 |
| ZnO | 1.610 | 1.550 | 1.370 | 0.980 | 1.462 | 1.401 | 1.138 | 1.113 | 1.125 | 0.305 | 0.780 | 0.570 | 0.620 |
| NiO | 0 | 0 | 0.010 | 0.120 | 0.018 | 0.035 | 0.217 | 0.307 | 0.172 | 0.089 | 0.120 | 0 | 0 |
| $Na_2O$ | 0.060 | 0.080 | 0.110 | 0 | 0.136 | 0.118 | 0.220 | 0.293 | 0.315 | 0.042 | 0.040 | 0 | 0.020 |
| $K_2O$ | 0.030 | 0.010 | 0 | 0 | 0 | 0 | 0.000 | 0.000 | 0.007 | 0.000 | 0.010 | 0 | 0.010 |
| Cation Calculation (Oxygen: 4) (apfu) | | | | | | | | | | | | | |
| Si | 0 | 0.002 | 0 | 0.001 | 0.001 | 0 | 0.001 | 0.001 | 0.001 | 0.001 | 0 | 0 | 0.001 |
| Ti | 0 | 0 | 0.001 | 0 | 0 | 0.001 | 0 | 0.001 | 0 | 0 | 0 | 0 | 0 |
| Al | 1.897 | 1.901 | 1.86 | 1.904 | 1.932 | 1.943 | 1.975 | 1.972 | 1.976 | 1.928 | 1.923 | 1.917 | 1.927 |
| Cr | 0.003 | 0.001 | 0.003 | 0.003 | 0.016 | 0.014 | 0.004 | 0.004 | 0.004 | 0.004 | 0.009 | 0.011 | 0.011 |
| V | 0 | 0 | 0 | 0 | 0 | 0 | 0 | 0 | 0 | 0 | 0 | 0 | 0 |
| $Fe^{3+}$ | 0.104 | 0.099 | 0.141 | 0.09 | 0.057 | 0.047 | 0.03 | 0.036 | 0.035 | 0.067 | 0.07 | 0.072 | 0.063 |
| $Fe^{2+}$ | 0.566 | 0.555 | 0.576 | 0.564 | 0.657 | 0.669 | 0.375 | 0.359 | 0.355 | 0.603 | 0.588 | 0.607 | 0.601 |
| Mn | 0.012 | 0.013 | 0.01 | 0.014 | 0.003 | 0.001 | 0.001 | 0.002 | 0.001 | 0.013 | 0 | 0.001 | 0.001 |
| Mg | 0.381 | 0.393 | 0.373 | 0.402 | 0.297 | 0.289 | 0.576 | 0.583 | 0.587 | 0.373 | 0.388 | 0.38 | 0.384 |
| Ca | 0 | 0.001 | 0.002 | 0 | 0 | 0 | 0 | 0 | 0 | 0 | 0 | 0.001 | 0 |
| Zn | 0.032 | 0.031 | 0.028 | 0.02 | 0.029 | 0.028 | 0.022 | 0.022 | 0.022 | 0.006 | 0.016 | 0.011 | 0.012 |
| Ni | 0 | 0 | 0 | 0.003 | 0 | 0.001 | 0.005 | 0.006 | 0.004 | 0.002 | 0.003 | 0 | 0 |
| Na | 0.003 | 0.004 | 0.006 | 0 | 0.007 | 0.006 | 0.011 | 0.015 | 0.016 | 0.002 | 0.002 | 0 | 0.001 |
| K | 0.001 | 0 | 0 | 0 | 0 | 0 | 0 | 0 | 0 | 0 | 0 | 0 | 0 |
| Σ cation | 2.999 | 3 | 3 | 3.001 | 2.999 | 2.999 | 3 | 3.001 | 3.001 | 2.999 | 2.999 | 3 | 3.001 |
| Mg/(Fe+Mg) | 0.402 | 0.414 | 0.393 | 0.416 | 0.311 | 0.302 | 0.605 | 0.619 | 0.623 | 0.382 | 0.397 | 0.385 | 0.390 |
| Ca/(Ca+Na+K) | 0.065 | 0.113 | 0.232 | 0.000 | 0.000 | 0.000 | 0.015 | 0.000 | 0.000 | 0.000 | 0.106 | 1.000 | 0.000 |
| Mg/(Fe+Mg+Ca+Mn) | 0.397 | 0.409 | 0.388 | 0.410 | 0.310 | 0.301 | 0.604 | 0.617 | 0.622 | 0.377 | 0.397 | 0.384 | 0.389 |
| $Fe^{2+}/(Mg^{2+}+Fe^{2+})$ | 0.598 | 0.586 | 0.607 | 0.584 | 0.689 | 0.698 | 0.395 | 0.381 | 0.377 | 0.618 | 0.603 | 0.615 | 0.610 |
| $Fe^{3+}/(Al^{3+}+Fe^{3+})$ | 0.052 | 0.050 | 0.071 | 0.045 | 0.029 | 0.024 | 0.015 | 0.018 | 0.017 | 0.034 | 0.035 | 0.036 | 0.031 |

| | | | | | **Magnetite** | | | | |
|---|---|---|---|---|---|---|---|---|---|
| Rock Type | **Cordierite Gneiss** | | **GBG** | | **Khondalite** | | **Migmatite** | | |
| Sample No | MP16 | | MA35 | | RS 1 | | MP-20 | | |
| Analysis No | 20 | 21 | 1 | 2 | 2 | 37 | 37 | 41 | 42 |
| $SiO_2$ | 0.032 | 0.073 | 0.066 | 0.087 | 0.000 | 0.160 | 0.180 | 0.060 | 3.920 |
| $TiO_2$ | 0.160 | 0.000 | 0.071 | 0.000 | 0.002 | 0.280 | 0.140 | 0.080 | 0.040 |
| $Al_2O_3$ | 0.319 | 0.356 | 0.537 | 0.379 | 0.045 | 2.340 | 2.520 | 0.290 | 3.000 |
| $Cr_2O_3$ | 0.129 | 0.060 | 0.117 | 0.104 | 0.000 | 0.080 | 0.120 | 0.130 | 0.070 |
| $FeO^t$ | 91.004 | 91.407 | 90.531 | 89.672 | 77.675 | 94.840 | 92.100 | 96.820 | 83.720 |
| MnO | 0.061 | 0.000 | 0.000 | 0.000 | 0.000 | 0.070 | 0.000 | 0.040 | 0.000 |
| MgO | 0.058 | 0.006 | 0.141 | 0.187 | 0.005 | 0.430 | 0.540 | 0.120 | 0.940 |
| CaO | 0 | 0 | 0 | 0 | 0.000 | 0.070 | 0.040 | 0.040 | 0.030 |
| ZnO | 0 | 0.049 | 0.043 | 0 | 0.029 | 0.000 | 0.000 | 0.000 | 0.000 |
| NiO | 0.039 | 0.171 | 0 | 0.060 | 0.760 | 0.000 | 0.140 | 0.000 | 0.290 |
| $Na_2O$ | 0.000 | 0.048 | 0 | 0.023 | 0.000 | 0.170 | 0.120 | 0.070 | 0.090 |
| $K_2O$ | 0.001 | 0.001 | 0.002 | 0.000 | 0.000 | 0.000 | 0.030 | 0.000 | 0.040 |
| Cation Calculation (Oxygen: 1) (apfu) | | | | | | | | | |
| Si | 0.001 | 0.003 | 0.003 | 0.003 | 0 | 0.006 | 0.007 | 0.002 | 0.148 |
| Ti | 0.005 | 0 | 0.002 | 0 | 0 | 0.008 | 0.004 | 0.002 | 0.001 |
| Al | 0.015 | 0.016 | 0.025 | 0.018 | 0.002 | 0.099 | 0.109 | 0.013 | 0.134 |
| Cr | 0.004 | 0.002 | 0.004 | 0.003 | 0 | 0.002 | 0.003 | 0.004 | 0.002 |
| V | 0 | 0 | 0 | 0 | 0 | 0 | 0 | 0 | 0 |
| $Fe^{3+}$ | 1.97 | 1.98 | 1.962 | 1.974 | 1.997 | 1.884 | 1.876 | 1.98 | 1.575 |
| $Fe^{2+}$ | 0.999 | 0.988 | 0.995 | 0.987 | 0.971 | 0.962 | 0.955 | 0.985 | 1.069 |
| Mn | 0.002 | 0 | 0 | 0 | 0 | 0.002 | 0 | 0.001 | 0 |
| Mg | 0.003 | 0 | 0.008 | 0.011 | 0 | 0.023 | 0.03 | 0.007 | 0.053 |
| Ca | 0 | 0 | 0 | 0 | 0 | 0.003 | 0.002 | 0.002 | 0.001 |
| Zn | 0 | 0.001 | 0.001 | 0 | 0.001 | 0 | 0 | 0 | 0 |
| Ni | 0.001 | 0.005 | 0 | 0.002 | 0.028 | 0 | 0.004 | 0 | 0.009 |
| Na | 0 | 0.004 | 0 | 0.002 | 0 | 0.012 | 0.009 | 0.005 | 0.007 |
| K | 0 | 0 | 0 | 0 | 0 | 0 | 0.001 | 0 | 0.002 |
| Σ cation | 3 | 2.999 | 3 | 3 | 2.999 | 3.001 | 3 | 3.001 | 3.001 |
| Mg/(Fe+Mg) | 0.003 | 0.000 | 0.008 | 0.011 | 0.000 | 0.023 | 0.030 | 0.007 | 0.047 |
| Ca/(Ca+Na+K) | 0.000 | 0.000 | 0.000 | 0.000 | 0.000 | 0.000 | 0.000 | 0.000 | 0.000 |
| Mg/(Fe+Mg+Ca+Mn) | 0.003 | 0.000 | 0.008 | 0.011 | 0.000 | 0.023 | 0.030 | 0.007 | 0.047 |
| $Fe^{2+}/ (Mg^{2+}+Fe^{2+})$ | 0.997 | 1.000 | 0.992 | 0.989 | 1.000 | 0.977 | 0.970 | 0.993 | 0.953 |
| $Fe^{3+}/(Al^{3+}+Fe^{3+})$ | 0.992 | 0.992 | 0.987 | 0.991 | 0.999 | 0.950 | 0.945 | 0.993 | 0.922 |

*major oxides in wt%; atoms per formula unit (apfu).

cation proportions (Table 1) and also end-members of spinel group minerals (Table 2) are calculated through the above mentioned application.

Table 2. End member composition of Spinel Group of Minerals from Metapelites of KKB.

| Sample No | | Analysis No | End Member components of Spinel Group of Minerals | | | | | | | | | | | | | |
|---|---|---|---|---|---|---|---|---|---|---|---|---|---|---|---|---|
| | | | Spinel SS | Hercynite | Galaxite | Gahnite | Magnesio-ferrite | Magnetite | Jacobsite | Franklinite | Trevorite | Magnesio-chromite | Chromite | Zinco-chromite | | Ulvöspinel |
| Spinel | MP16 | 22 | $MgAl_2O_4$ | $FeAl_2O_4$ | $MnAl_2O_4$ | $ZnAl_2O_4$ | $MgFe_2O_4$ | $FeFe_2O_4$ | $MnFe_2O_4$ | $ZnFe_2O_4$ | $NiFe_2O_4$ | $MgCr_2O_4$ | $FeCr_2O_4$ | $ZnCr_2O_4$ | $Mg_2TiO_4$ | $Fe_2TiO_4$ |
| | MA35 | 3 | 2.891 | 4.674 | 0.103 | 0.047 | 0.101 | 0.163 | 0.004 | 0.002 | 0.001 | 0.006 | 0.009 | 0 | 0.001 | 0.001 |
| | | 4 | 4.648 | 3.028 | 0.012 | 0.178 | 0.07 | 0.045 | 0 | 0.003 | 0.001 | 0.009 | 0.006 | 0 | 0.001 | 0 |
| | | 5 | 4.732 | 2.913 | 0.017 | 0.175 | 0.087 | 0.054 | 0 | 0.003 | 0.001 | 0.009 | 0.005 | 0 | 0.001 | 0.001 |
| | RS1 | 3 | 4.771 | 2.887 | 0.009 | 0.178 | 0.085 | 0.051 | 0 | 0.003 | 0.001 | 0.01 | 0.006 | 0 | 0 | 0 |
| | | 4 | 2.32 | 5.137 | 0.021 | 0.23 | 0.068 | 0.151 | 0.001 | 0.007 | 0 | 0.019 | 0.043 | 0.002 | 0 | 0 |
| | MP-20 | 35 | 2.27 | 5.251 | 0.01 | 0.221 | 0.055 | 0.128 | 0 | 0.005 | 0 | 0.016 | 0.037 | 0.002 | 0.001 | 0.002 |
| | | 36 | 2.912 | 4.323 | 0.09 | 0.247 | 0.16 | 0.238 | 0.005 | 0.014 | 0 | 0.004 | 0.006 | 0 | 0 | 0 |
| | | 39 | 3.01 | 4.251 | 0.1 | 0.237 | 0.157 | 0.222 | 0.005 | 0.012 | 0 | 0.002 | 0.003 | 0 | 0 | 0 |
| | | 40 | 2.808 | 4.327 | 0.077 | 0.21 | 0.213 | 0.329 | 0.006 | 0.016 | 0 | 0.004 | 0.006 | 0 | 0.001 | 0.002 |
| | ERKM | 2 | 3.066 | 4.307 | 0.103 | 0.149 | 0.145 | 0.204 | 0.005 | 0.007 | 0.001 | 0.005 | 0.007 | 0 | 0 | 0 |
| | | 6 | 3.006 | 4.554 | 0 | 0.121 | 0.11 | 0.167 | 0 | 0.004 | 0.001 | 0.014 | 0.021 | 0.001 | 0 | 0 |
| | | 8 | 2.916 | 4.654 | 0.011 | 0.088 | 0.109 | 0.174 | 0 | 0.003 | 0 | 0.017 | 0.027 | 0.001 | 0 | 0 |
| Magnetite | MP16 | 20 | 2.964 | 4.641 | 0.005 | 0.096 | 0.096 | 0.151 | 0 | 0.003 | 0 | 0.017 | 0.026 | 0.001 | 0 | 0 |
| | | 21 | 0 | 0.058 | 0 | 0 | 0.027 | 7.854 | 0.016 | 0 | 0.01 | 0 | 0.016 | 0 | 0 | 0.019 |
| | MA35 | 1 | 0 | 0.065 | 0 | 0 | 0.003 | 7.871 | 0 | 0.011 | 0.043 | 0 | 0.007 | 0 | 0 | 0 |
| | | 2 | 0.001 | 0.098 | 0 | 0 | 0.064 | 7.804 | 0 | 0.01 | 0 | 0 | 0.014 | 0 | 0 | 0.008 |
| | RS 1 | 2 | 0.001 | 0.07 | 0 | 0 | 0.087 | 7.814 | 0 | 0 | 0.015 | 0 | 0.013 | 0 | 0 | 0 |
| | MP-20 | 37 | 0 | 0.009 | 0 | 0 | 0.003 | 7.757 | 0 | 0.008 | 0.223 | 0 | 0 | 0 | 0 | 0 |
| | | 38 | 0.009 | 0.387 | 0.001 | 0 | 0.176 | 7.371 | 0.016 | 0 | 0 | 0 | 0.009 | 0 | 0.001 | 0.03 |
| | | 41 | 0.013 | 0.423 | 0 | 0 | 0.225 | 7.277 | 0 | 0 | 0.032 | 0 | 0.014 | 0 | 0 | 0.015 |
| | | 42 | 0 | 0.05 | 0 | 0 | 0.052 | 7.864 | 0.01 | 0 | 0 | 0 | 0.015 | 0 | 0 | 0.009 |
| | | 42 | 0.029 | 0.59 | 0 | 0 | 0.345 | 6.963 | 0 | 0 | 0.057 | 0 | 0.009 | 0 | 0 | 0.005 |

# $MnCr_2O_4$, $NiCr_2O_4$, $MgV_2O_4$, $FeV_2O_4$, $MnV_2O_4$ for all the samples are 0.00

### 4.1. Spinel

The spinel found in the examined rock samples exhibits compositional differences based on its specific setting and structural relationship, yet it predominantly exists as a solid solution of hercynite. The general formula of the spinel group of minerals is X $Y_2$ $O_4$, where X represent $Mg^{2+}$, $Fe^{2+}$, Zn, Mn and Ni and Y represents $Al^{3+}$, $Fe^{3+}$ and $Cr^{3+}$. The Spinel group was further subdivided into three series as per the trivalent cation in Y site (Deer et al., 1972). These are Spinel series ($Al^{3+}$), Magnetite series ($Fe^{3+}$) and Chromite series ($Cr^{3+}$). Among them, the spinel from the rocks of the study area of KKB are marked as Al-rich spinel (Fig. 4) and show a granulite facies metamorphic condition. As per the binary classification diagram (Deer et al., 1972) for spinel group of minerals, the spinel from KKB falls under the intermediate pleonaste variety with varying amounts of $Fe^{2+}$ from south to north (Fig. 5). The EPMA data clearly show that spinel is rich in $Al_2O_3$, FeO, and MgO. $Al_2O_3$ and MgO content of spinel varies in order from 57.06 to 63.76 wt%, 17.74 to 31.41 wt% and 7.11 to 14.97 wt% respectively (Table 1). The ZnO content in the spinel samples vary from 1.6 to 0.32 wt% (Fig. 5, Table 1). Overall the $Cr_2O_3$ content is low in spinel and the value ranges from 0.06 to 0.7 wt%. The $Fe^{3+}$ versus Al as well as $Fe^{2+}$ versus Mg binary plots (Fig. 6a and 6b) for spinel from the study area indicates that the $Al^{3+}$–$Fe^{3+}$ and $Mg^{2+}$–$Fe^{2+}$ substitutions are also common in the spinel.

### 4.2. Magnetite

Magnetite in the studied sample occurs as an accessory mineral phase in the metapelites and is found both in the ground mass and as well as within inclusion within garnet and cordierite. In most cases, magnetite is found to be sharing boundary with spinel. They are generally anhedral crystals of varying size and shape. Magnetite occurs as patches within spinel as well as more developed grain sharing boundary with spinel (Fig. 3a, 3b). The total FeO content ranges from 96.82 to 77.67 wt%. Magnetite shows Al-poor nature and varies from 0.045 to 3.0 wt%. The $Cr_2O_3$ and $TiO_2$ content in the magnetite varies from 0.06 to 0.13 wt% and 0.04 to 0.28 wt%.

### 4.3. Compositional diversity of Spinel and Magnetite

The end member composition (Table 2) of spinel group of minerals shows significant variation in the composition, even within the same sample location (e.g., MP-16). This suggests the presence of multiple spinel phases present in the area. Across most of the spinel analysis, the hercynite ($FeAl_2O_4$) end-member shows the highest mole percentages. This indicates that the dominant chemical composition of these spinel grains is iron-aluminum oxide. Samples MA35 and MP-20, show appreciable amounts of gahnite ($ZnAl_2O_4$). This suggests the presence of zinc in the metamorphic environment where these spinel formed. The variation in gahnite content within and between samples could reflect local variations in zinc availability. While hercynite is dominant, there's a consistent presence of the spinel Sensu Stricto ($MgAl_2O_4$) end-member (magnesium aluminium oxide), indicating a solid solution between hercynite and spinel. The percentages of chromite ($FeCr_2O_4$) and ulvöspinel ($Fe_2TiO_4$) are generally very low or absent in these spinel. This suggests that chromium and titanium were not major components in the formation of these aluminium-rich spinel. The almandine spinel ($MnAl_2O_4$) end-member is present in very small amounts in some analysis. The concentration of ZnO in metapelitic rocks plays a crucial role in their thermal history and mineral transformations. ZnO

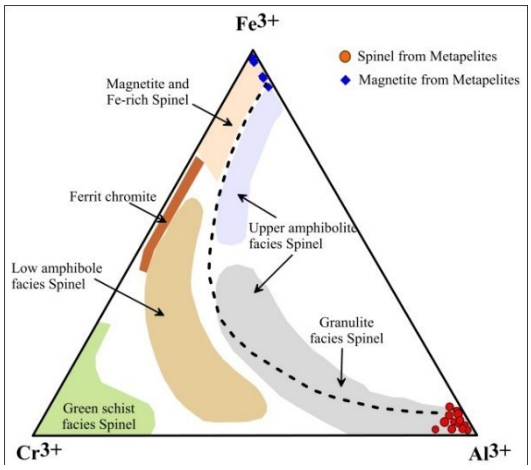


Fig. 4. $Fe^{3+}$–$Cr^{3+}$–$Al^{3+}$ triangular plot (after Saumur and Hattori, 2013) for spinel and magnetite from southern KKB.

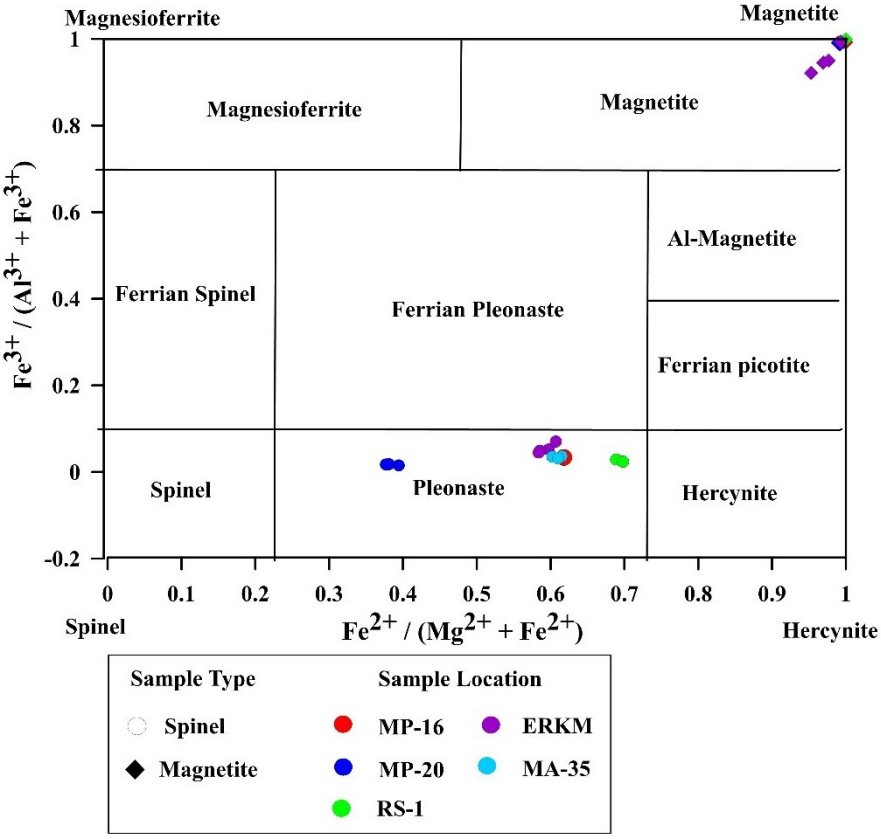


Fig. 5. Classification diagram for spinel group of minerals (after Deer et al., 1972) from metapelites of KKB.

content in the spinel vary from 0.305 to 1.16 wt%. (Table 1).

In the end-member calculation, the magnetite ($Fe\ O_4$) end-member is overwhelmingly dominant in analyses of magnetite grains (Table 2). This confirms that these grains are primarily composed of iron oxide with a spinel structure. Moreover there is a notable presence of the ulvöspinel ($Fe_2TiO_4$) end-member. This indicates the substitution of titanium into the magnetite structure, forming a solid solution series. The presence of both magnetite and ulvöspinel indicate oxidation of an initial titanomagnetite solid solution, potentially leading to exsolution textures. The other end-members like hercynite, gahnite, and chromite are generally present in very low or trace amounts in the magnetite grains. This suggests that aluminum, zinc, and chromium were not readily incorporated into the magnetite structure under these conditions.

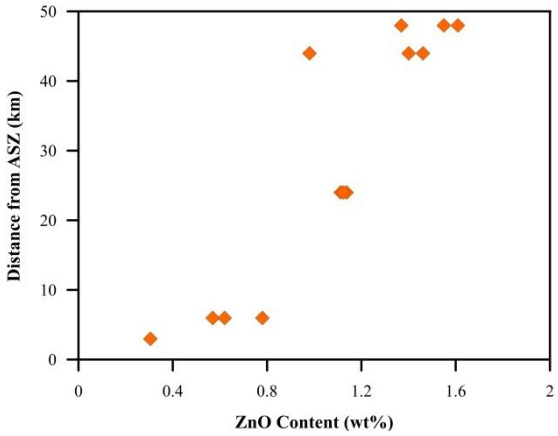


Fig. 6. ZnO content variation in the spinel concerning distance from ASZ.

### 4.4. Garnet–Cordierite geothermobarometers.

The Garnet–Cordierite geothermometer of Bhattacharya et al. (1988) was applied to estimate the retrograde conditions as cordierite is texturally a product of retrograde metamorphism. Application of this method to cordierite and adjacent garnet (rim) yielded a temperature range of 731–735 °C (MP-16) and 745–751 °C (MA-35) at 4 kbar. The ranges obtained from the methods of Holdaway and Lee (1977) and Nichols et al. (1992) are about 50–75 °C lower than those from Bhattacharya et al. (1988), but the calculated results from the three methods are almost consistent. Application of an experimental geobarometer of Nichols et al. (1992) yielded a nearly consistent pressure range of 4.62–4.77 kbar at 640 °C. Similar observation based on textural studies were drawn by John and Nandakumar (2025) from the KKB recently.

## 5. Discussion

Based on the petrographic and mineralogical data the mode of occurrence and coexistence of spinel and magnetite in the KKB are notably distinct, as evidenced by both field observations and petrographic analyses. As per $Fe^{3+}$, $Al^{3+}$ and $Cr^{3+}$ ternary discrimination plot (after Saumur and Hattori, 2013) all the spinel from the study area falls under the granulite facies metamorphic zone (Fig. 4). According to Cesare (1994), hercynite formation is characteristic of low-pressure, high-temperature conditions within the granulite or upper amphibolite facies of regional and contact metamorphism. In these environments, hercynite is typically produced by the reaction of iron-rich cordierite with surrounding aluminum-silicate rocks. The occurrence of garnet rimmed by spinel, or vice versa, is indicative of reaction boundaries that may result from partial retrogression or incomplete metamorphic reactions. Such textures are characteristic of disequilibrium conditions during metamorphism. Specifically, reaction-rim (corona, Fig. 2f) textures form due to mineral reactions under varying metamorphic conditions, including pressure, temperature, fluids, and stress. These textures provide insights into the progressive or retrogressive evolution between different generations of minerals at grain boundaries (Prakash et al., 2014).

In this study, none of the spinel shows typical hercynite composition and all are in transition phase in pleonaste with hercynite end-member as highest mole percentages (Table 1). Moreover, the Zn content in spinel is thought to be derived from Zn-rich biotite, as Zn can readily substitute for $Fe^{2+}$ during granulite facies metamorphism. The occurrence of spinel–quartz assemblages typically indicates temperature-dominated metamorphism (Barbosa et al., 2006) and may also signify ultra-high temperature (UHT) conditions (Morimoto et al., 2004). Nichols et al. (1992) noted that higher zinc (Zn) content in spinel coexisting with quartz lowers its stability temperature. Metapelites, which are metamorphosed clay-rich sedimentary rocks, undergo complex mineralogical changes under varying pressure and temperature conditions. ZnO influences the stability and formation of spinel, garnet, and other aluminous minerals during metamorphism. Studies indicate that spinels in granulites can be classified into Zn-poor (<3 wt% ZnO) and Zn-bearing (7–20 wt% ZnO) varieties, with some reaching up to 30 wt% ZnO. (Baba et al., 2019) The presence of ZnO influences the stability of spinel and its transformation into other mineral phases, such as garnet and magnetite. In the Eastern

 

Ghats Belt, India, spinel granulites exhibit Zn-rich spinel compositions, particularly in sapphirine-absent domains, where ZnO plays a role in mineral reactions and retrograde metamorphism (Dasgupta et al., 1995). Additionally, compositional studies from Digapahandi suggest that ZnO variations in spinel are linked to high-temperature metamorphic conditions (Misra and Vishwakarma, 2018).

Similarly, Santosh et al. (2006) proposed that low-Zn spinel in equilibrium with quartz form at UHT conditions, whereas high-Zn spinel forms during the retrograde (cooling and decompression) metamorphic stage. The ZnO content in the spinel samples varies from 0.305 to 1.61 wt% clearly showing they are Zn-poor variety. To understand the effect of major lineament the distance from the ASZ is calculated and plotted against the ZnO concentration in the spinel to identify any such relation exists shows a positive correlation between the two. Here an increasing trend away from the ASZ (Table 1, Fig. 6). The concentration of ZnO in spinel is mostly controlled by the thermodynamic condition of the area. Similarly, the presence of high magnesium content in spinel in the central part indicates a higher grade of metamorphism for localised parts of KKB.

In this study, magnetite is observed in close association with spinel. Magnetite occur as exsolution patches within the spinel grains and also in equilibrium with the spinel (Fig. 2, 3). Ramdohr (1969), in his influential work on ore microscopy, documented exsolution textures within iron–magnesium–zinc–aluminum (Fe–Mg–Zn–Al) spinel. His observations reveal that these complex spinel, initially formed at high temperatures, can incorporate significant amounts of ferric iron ($Fe^{3+}$) into their crystal structure, resulting in the formation of solid solutions. However, upon cooling, the solubility of $Fe^{3+}$ in spinel decreases, leading to the exsolution of distinct iron oxide phases such as magnetite (Fe $O_4$) or hematite ($Fe_2O$ ). These phases appear as microscopic features—thin lamellae, irregular blebs, or fine-grained networks—within or along the boundaries of the original spinel grains. This phenomenon suggests that spinel with higher initial $Fe^{3+}$ content is more susceptible to unmixing during retrograde cooling. This is clear in the BSE images (see Fig. 3c). Based on the above study, it can be concluded that the diverse composition of spinel–magnetite assemblages in the metapelites of the KKB is not solely due to variations in bulk rock composition, but also reflects the differing metamorphic conditions the rocks have experienced. The low Fe content in spinel associated with magnetite suggests the possible exsolution of magnetite from spinel during cooling, as noted by Ramdohr (1969).

The relationship between $Al^{3+}$ and $Fe^{3+}$ (Fig. 7) shows a negative correlation in the spinel chemistry reflects a substitution mechanism where $Fe^{3+}$ replaces $Al^{3+}$ in the spinel structure (Andreozzi and Lucchesi, 2002). Indicates increasing oxidation state during metamorphism. Spinel adjusting to changing redox conditions might signify reaction rims or re-equilibration in response to $Fe^{3+}$ enrichment as evident from the petrographic studies. A negative trend $Mg^{2+}$ decreases as $Fe^{2+}$ increases is observed in the spinel indicates $Fe^{2+}$–$Mg^{2+}$ substitution, typical of solid solution between spinel components (e.g., $MgAl_2O_4$–$FeAl_2O_4$). Whereas most magnetite data cluster around $Fe^{3+}$, with low other cation value reflects magnetite's ideal formula ($Fe^{2+}Fe^{3+}{}_2O_4$), which structurally favours high $Fe^{3+}$ content. The consistency with near-endmember magnetite supports high redox stability except samples from ERKM (Fig. 7). This points that the magnetite of ERKM samples reflect minor substitution or exsolution processes, possibly linked to spinel exsolution (Fig. 3a, 3b).

The textural relationship different mineral in the GBG and cordierite gneiss preserve signatures of both prograde and retrograde metamorphic trend clearly indicate a polyphase metamorphim experienced in the rocks of KKB. The Garnet - Cordierite geothermometer applied to the cordierite with retrograde textural signature and adjacent garnet yielded a temperature range of 731–750 °C nearly consistent pressure range of 4.62–4.77 kbar.

## 6. Conclusions

This study provides a detailed investigation into the spinel–magnetite associations within high-grade metapelites of the KKB, elucidating their petrogenetic significance in the context of regional metamorphism.

- The mineral assemblage (spinel, cordierite, sillimanite, garnet, plagioclase and magnetite) in the cordierite gneiss, migmatite and GBG indicate that rocks of KKB experienced a high-temperature metamorphism, likely in the granulite facies.

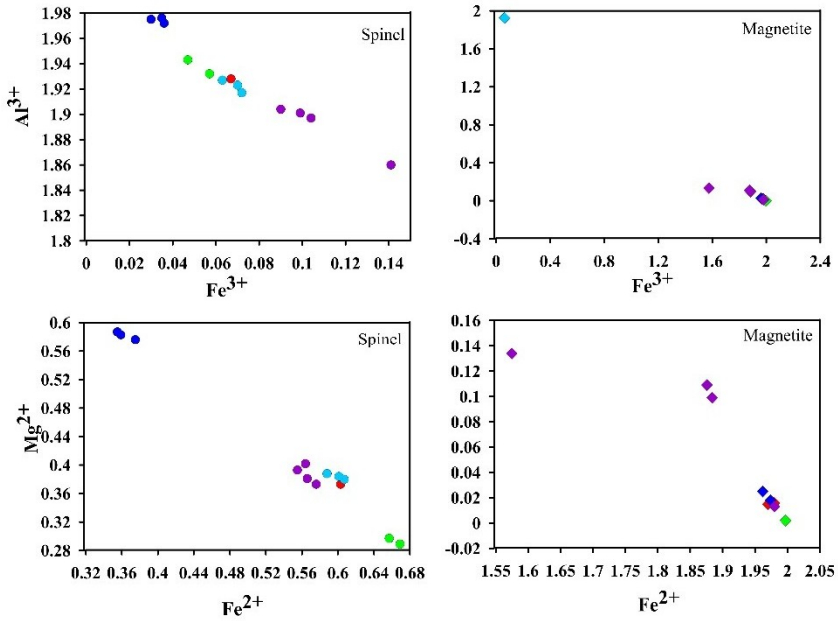


Fig. 7. Binary plot for the spinel and magnetite from the KKB (a) $Al^{3+}$ vs. $Fe^{3+}$ plot (b) $Mg^{2+}$ vs. $Fe^{2+}$ plot. Symbol index is same as that of Fig. 5.

- Electron Probe Microanalysis (EPMA) data shows that spinel in the KKB rocks are aluminum-rich and classified as intermediate pleonaste, with varying $Fe^{2+}$ content.
- Spinel is Al-rich and Cr-poor, suggesting formation in metapelites under dry, high-temperature conditions.
- Spinel often occurs intergrown with cordierite and in contact with garnet or magnetite and Magnetite is observed along margins of spinel, within garnet and as inclusions in other minerals. This suggests redox-controlled breakdown or formation reactions, consistent with oxidation of $Fe^{2+}$ to $Fe^{3+}$ and formation of magnetite during decompression or cooling.
- ZnO content in the spinel samples generally shows an increasing trend away from the Achankovil Shear Zone. The association of spinel–quartz assemblages suggest temperature-dominated regional metamorphism, potentially including ultra-high temperature conditions and a retrograde metamorphic stage.
- Spinel shows significant cation exchange ($Fe^{3+}\leftrightarrow Al^{3+}$ and $Fe^{2+}\leftrightarrow Mg^{2+}$), indicative of dynamic metamorphic conditions, such as partial retrogression or reaction rims around garnet. Magnetite, being chemically simpler and more oxidized, appears to be either a later phase, or a redox partner in reactions involving spinel or garnet breakdown. This geochemical evidence strengthens textural interpretations—especially regarding garnet-spinel-magnetite associations as metamorphic reaction products tied to oxidation state shifts during granulite to retrograde condition.
- Even though, this study describes the association of spinel-magnetite from the KKB, the detailed oxygen isotope studies on garnet–spinel–magnetite assemblages to evaluate the role of fluid infiltration and redox buffering during retrogression and zircon U–Pb dating from the same samples could establish the timing of peak and retrograde metamorphism, integrating the thermal history with tectonic events. By integrating these future approaches with the present dataset, a more complete picture of the metamorphic and tectonic evolution of the KKB - and its broader implications for southern Indian crustal architecture can be developed.

## Acknowledgements

The authors are thankful to KSCSTE, Thiruvananthapuram, for partial financial support of the research work. They are also thankful to the Head of

 

the Department of Geology for lab facilities. The authors would like to thank ADG & HOD, N.R., GSI, for the encouragement and support in publishing this work. We are also grateful to the Centre of Excellence EPMA Lab, GSI, Kolkata, for their kind assistance on microprobe analysis.

## Conflict of interest

We wish to confirm that there are no known conflicts of interest associated with this publication and there has been no significant financial support for this work that could have influenced its outcome.

## CRediT statement

**Resmi S**: Conceptualization, Data curation, Methodology, Validation, Software, Investigation, Writing – original draft. **Shaji E**: Conceptualization, Supervision, Methodology, Validation Writing – review & editing. **Dhanil Dev S.G.**: Data curation, Methodology, Validation.

## References

Andreozzi, G.B., Lucchesi, S., 2002. Intersite distribution of $Fe^{2+}$ and Mg in the spinel (sensu stricto)–hercynite series by single-crystal X-ray diffraction. *American Mineralogist* 87(8-9), 1113–1120. https://doi.org/10.2138/am-2002-8-908.

Atkin, B.P., 1978. Hercynite as a breakdown product of staurolite from within the aureole of the Ardara pluton, Co. Donegal, Eire. *Mineralogical Magazine* 42, 237–239. https://doi.org/10.1180/minmag.1978.042.322.10.

Aung, W.Y.L., Nyunt, T.T., 2021. The existence of hercynite in metapelites from Mogok Metamorphic Belt. *Journal of Myanmar Academy of Arts and Science* 19(5A), 271–280.

Baba, S., Osanai, Y., Adachi, T., Nakano, N., Hokada, T., Toyoshima, T., 2019. Metamorphic P-T conditions and variation of REE between two garnet generations from granulites in the Sør-Rondane mountains, East Antarctica. *Mineralogy and Petrology* 113, 821–845. https://doi.org/10.1007/s00710-019-00680-0.

Barbosa, J., Nicollet, C., Leite, C., Kienast, J.R., Fuck, R.A., Macedo, E.P., 2006. Hercynite-quartz-bearing granulites from Brejes Dome area, Jequi Block. *Lithos* 92, 537–556,. https://doi.org/10.1016/j.lithos.2006.03.064.

Bhattacharya, A., Mazumdar, A.C., Sen, S.K., 1988. Fe–Mg mixing in cordierite: constraints from natural data and implications for cordierite–garnet geothermometry in granulites. *American Mineralogist* 73, 338–344.

Bindu, R.S., Suzuki, K., Yoshida, M., Santosh, M., 1998. The first report of CHIME monazite age from the south Indian granulite terrain. *Current Science* 74, 852–858.

Braun, I., Raith, M., R.G.R, Kumar, 1996. Dehydration melting phenomena in leptynitic gneiss and the generation of leucogranites: a case study from the Kerala Khondalite Belt, Southern India. *Journal of Petrology* 37, 1285–1305. https://doi.org/10.1093/petrology/37.6.1285.

Cenki, B., Braun, I., Brocker, M., 2004. Evolution of the continental crust in the Kerala Khondalite Belt, southernmost India: evidence from Nd isotope mapping, U–Pb and Rb–Sr geochronology. *Precambrian Research* 134(3–4), 275–292. https://doi.org/10.1016/j.precamres.2004.06.002.

Cesare, B., 1994. Hercynite as the product of staurolite decomposition in the contact aureole of Vedrette di Ries, eastern Alps, Italy. *Contributions to Mineralogy and Petrology* 116, 239–246,. https://doi.org/10.1007/BF00306495.

Chacko, T., Kumar, R.G.R., Newton, R.C., 1987. Metamorphic P-T conditions of the Kerala (south India) Khondalite Belt: a granulite facies supracrustal terrain. *Journal of Geology* 96, 343–358. https://doi.org/10.1086/629134.

Dasgupta, S., Sengupta, P., Ehl, J., Raith, M., Bardhan, S., 1995. Reaction textures in a suite of spinel granulites from the Eastern Ghats Belt, India: Evidence for polymetamorphism, a partial petrogenetic grid in the system KFMASH and the roles of ZnO and Fe2O3. *Journal of Petrology* 36(2), 435–461. https://doi.org/10.1093/petrology/36.2.435.

Deer, W.A., Howie, R.A., Zussman, J., 1972. *Rock forming minerals Vol.1, ortho- and ring-silicates*. Longman Group Ltd, London, England. https://doi.org/10.1180/DHZ.

Droop, G.T.R., 1987. A General equation for estimating Fe3+ concentrations in ferromagnesian silicates and oxides from microprobe analyses, using stoichiometric criteria. *Mineralogical Magazine* 51, 431–435. https://doi.org/10.1180/minmag.1987.051.361.10.

Ferracutti, G.R., Gargiulo, M.F., Ganuza, M.L., Bjerg, E.A., Castro, S.M., 2015. Determination of the spinel group end-members based on electron microprobe analyses. *Mineralogy and Petrology* 109(2), 153–160. https://doi.org/10.1007/s00710-014-0363-1.

Frost, B.R., 1973. Ferroan gahnite from quartz-biotite-almandine schist, Wind River Mountains, Wyoming. *American Mineralogist* 58, 831–834.

Harley, S.L., 1998. *On the occurrence and characterisation of ultrahigh-temperature crustal metamorphism*. Geological Society of London Special Publication. https://doi.org/10.1144/GSL.SP.1996.138.01.06.

Herd, R.K., Ackermand, D., Thomas, A., Windley, A., 1987. Oxygen fugacity variations and mineral reactions in sapphirine-bearing paragneisses, E. Grenville province, Canada. *Mineralogical Magazine* 51(360), 203 – 206. https://doi.org/10.1180/minmag.1987.051.360.02.

Holdaway, M.J., Lee, S.M., 1977. Fe–Mg cordierite stability in high-grade politic rocks based on experimental, theoretical, and natural observations. *Contributions to Mineralogy and Petrology* 63, 175–198. https://doi.org/10.1007/BF00398778.

John, A.J., Nandakumar, V., 2025. Reaction textures and metamorphic evolution of spinel-bearing metapelites of Kerala Khondalite Belt, Southern Granulite Terrain, India. *Journal of Geointerface* 4(1), 68–82. https://doi.org/10.5281/zenodo.15569357.

Kadowaki, H., Tsunogae, T., He, X., Santosh, M., Takamura, Y., Shaji, E., Tsutsumi, Y., 2019. Pressure-temperature-time evolution of ultrahigh-temperature granulites from the Trivandrum Block, southern India: Implications for long-lived high-grade metamorphism. *Geological Journal* , 1–19. https://doi.org/10.1002/gj.3422.

 

Kumar, R.G., Sreejith, C., 2016. Petrology and geochemistry of charnockites (felsic ortho-granulites) from the Kerala Khondalite Belt, Southern India: evidence for intra-crustal melting, magmatic differentiation and episodic crustal growth. *Lithos* 262, 334–54. https://doi.org/10.1016/j.lithos.2016.07.009.

Kumar, R.G.R., Srikantappa, C., Hansen, E., 1985. Charnockite formation at Ponmudi, Kerala, South India. *Nature* 313, 207–209. https://doi.org/10.1038/313207a0.

Loomis, T.P., 1972. Contact metamorphism of pelitic rock by the Ronda ultramafic inclusion, southern Spain. *Geological Society of America Bulletin* 83, 2449–2474. https://doi.org/10.1130/0016-7606(1972)83.

Mahanta, B., Prakash, D., M., Kumar, Singh, S., Pandey, R.K., Singh, C.K., Yadav, R., Vinas, J.S., 2025. Ultrahigh temperature granulites from the Shillong–Meghalaya Gneissic Complex, NE India: Implications for the Indo–Antarctic Correlation. *Journal of Asian Earth Sciences* 279, 106461. https://doi.org/10.1016/j.jseaes.2024.106461.

Misra, S., Vishwakarma, N., 2018. Compositional variation of Spinel from metamorphic rocks of Digapahandi area, Eastern Ghats Belt, India. *Journal of Applied Geology and Geophysics (IOSR-JAGG)* 6(4), 21–27. https://doi.org/10.9790/0990-0604012127.

Morimoto, T., Santosh, M., Tsunogae, T., Yoshimura, Y., 2004. Spinel + Quartz association from the Kerala khondalites, southern India: evidence for ultrahigh temperature metamorphism. *Journal of Mineralogical and Petrological Sciences* 99, 257–278. https://doi.org/10.2465/jmps.99.257.

Nandakumar, V., Harley, S.L., 2000. A reappraisal of the pressure-temperature path of granulites from the Kerala Khondalite Belt, Southern India. *Journal of Geology* 108(6), 687–703. https://doi.org/10.1086/317947.

Navrotsky, A., Kleppa, O.J., 1968. Thermodynamics of formation of simple spinel. *Journal of Inorganic and Nuclear Chemistry* 30, 479–498. https://doi.org/10.1016/0022-1902(68)80475-0.

Nichols, G.T., Berry, R.F., Green, D.H., 1992. Internally consistent gahnitic spinel-cordierite-garnet equilibria in the FMASHZN system: Geothermobarometry and applications. *Contributions to Mineralogy and Petrology* 111, 362–377. https://doi.org/10.1007/BF00311197.

Nugumanova, Y., Doroshkevich, A., Starikova, A., Garcia, J., 2024. Composition of olivines and spinel group minerals in aillikites from the Bushkanay dyke, South Siberian Craton: Insights into alkaline melt sources and evolution. *Geosystems and Geoenvironment* 3(4), 100247. https://doi.org/10.1016/j.geogeo.2023.100247.

Ouzegane, K., Linnemann, U., Gartner, A., Doukkari, S., Arab, A., Drareni, A., Kienast, J.R., Bendaoud, A., 2025. Geochronology and P-T paths of metapelites and garnet pyroxenites from Tamanrasset Block (Central Hoggar, Algeria): Evidence of a Neoproterozoic deposition and high-grade metamorphism, in: Hamoudi, M., Bendaoud, A., Bodinier, J.L., Ouzegane, K., Perfettini, H. (Eds.), *Lithospheric Architecture and Precambrian Geology of the Hoggar and Adjacent Areas.* Regional Geology Reviews. Springer, Cham. https://doi.org/10.1007/978-3-319-70250-6_4.

Power, M.R., Pirrie, D., Andersen, J.C., Wheeler, P.D., 2000. Testing the validity of chrome spinel chemistry as a provenance and petrogenetic indicator. *Geology* 28, 1027–1030. https://doi.org/10.1130/0091-7613(2000)28.

Prakash, D., Deepak, Singh, C., P., Singh, C.K., Tewari, S., Arima, M., Frimmel, H.E., 2014. Reaction textures and metamorphic evolution of sapphirine–spinel-bearing and associated granulites from Diguva Sonaba, Eastern Ghats Mobile Belt, India. *Geological Magazine* 152(02), 316–340. https://doi.org/10.1017/s0016756814000399.

Ramakrishnan, M., 1993. Tectonic evolution of the granulite terrains of southern India. *Geological Society of India Memoir* 25, 35–44. https://doi.org/10.1180/0680218.

Ramdohr, P., 1969. The Ore Minerals and their Intergrowths. *Pergamon Press* 1171p. https://doi.org/10.1016/C2013-0-10027-X.

Santosh, M., Morimoto, T., Tsutsumi, Y., 2006. Geochronology of the khondalite belt of Trivandrum Block, Southern India: Electron probe ages and implications for Gondwana tectonics. *Gondwana Research* 9, 261–278. https://doi.org/10.1016/j.gr.2005.11.003.

Saumur, B.M., Hattori, K., 2013. Zoned Cr-spinel and ferritchromite alteration in forearc mantle serpentinites of the Rio San Juan Complex, Dominican Republic. *Mineralogical Magazine* 77(1), 117–136. https://doi.org/10.1180/minmag.2013.077.1.11.

Shimizu, H., Tsunogae, T., Santosh, M., 2009. Spinel + quartz assemblage in granulites from the Achankovil Shear Zone, southern India: Implications for ultrahigh-temperature metamorphism. *Journal of Asian Earth Sciences* 36, 209–222. https://doi.org/10.1016/j.jseaes.2009.06.005.

Srikantappa, C., Raith, M., B, Spiering, 1985. Progressive charnockitization of a leptynite- khondalite suite in Southern Kerala, India- Evidence for the formation of charnockites through decrease in fluid pressure? *Journal of Geological Society of India* 26, 849–872. https://doi.org/10.17491/jgsi/1985/261201.

Tadokoro, H., Tsunogae, T., Santosh, M., 2008. Metamorphic P-T path of the eastern Trivandrum Granulite Block, southern India: implications for regional correlation of lower crustal fragments. *Journal of Mineralogical and Petrological Sciences* 103, 279–284. https://doi.org/10.2465/jmps.080110.

Tadokoro, H., Tsunogae, T., Santosh, M., Yoshimura, Y., 2007. First report of the spinel + quartz assemblage from Kodaikanal in the Madurai Block, southern India: Implications for ultrahigh-temperature metamorphism. *International Geology Review* 49, 1050–1068. https://doi.org/10.2747/0020-6814.49.11.1050.

Tajčmanová, L., Konopásek, J., Košler, J., 2009. Distribution of zinc and its role in the stabilization of spinel in high-grade felsic rocks of the Moldanubian domain (Bohemian Massif). *European Journal of Mineralogy* 21(2), 407–418. https://doi.org/10.1127/0935-1221/2009/0021-1899.

Wagner, M.E., Crawford, M.L., 1975. Polymetamorphism of the Precambrian Baltimore Gneiss in southeastern Pennsylvania. *American Journal of Science* 275(6), 653–682. https://doi.org/10.2475/ajs.275.6.653.

Wang, B., Wei, C.J., Tian, W., 2021. Evolution of spinel-bearing ultrahigh-temperature granulite in the Jining complex, North China Craton: constrained by phase equilibria and Monte Carlo methods. *Mineralogy and Petrology* 115, 283–297. https://doi.org/10.1007/s00710-021-00743-1.

 